Scaling all-fiber mid-infrared supercontinuum up to 10 W-level based on thermal-spliced silica fiber and ZBLAN fiber

Zhijian Zheng, Deqin Ouyang, Junqing Zhao, Minqiu Liu, Shuangchen Ruan,* Peiguang Yan, and Jinzhang Wang

Shenzhen Key Laboratory of Laser Engineering, Key Laboratory of Advanced Optical Precision Manufacturing Technology of Guangdong Higher Education Institutes, College of Optoelectronic Engineering, Shenzhen University, Shenzhen 518060, China

**Corresponding author: scruan@szu.edu.cn*

Received April 15, 2016; revised May 23, 2016; accepted May 24, 2016; posted May 26, 2016 (Doc. ID 263261); published June 22, 2016

We demonstrate an integrated all-fiber mid-infrared (mid-IR) supercontinuum (SC) source generated by a 1.95 μm master oscillator power amplifier system and a single-mode ZBLAN (ZrF_4–BaF_2–LaF_3–AlF_3–NaF) fiber. The maximum average output power is 10.67 W with spectral bandwidth covering from ~1.9 to 4.1 μm. The single-mode ZBLAN fiber and silica fiber are thermal-spliced to enhance the robustness and practicability of the system. It is, to the best of our knowledge, the first high-power integrated compacted all-fiber mid-IR SC source based on thermal-spliced silica fiber and ZBLAN fiber.

OCIS codes: (320.6629) Supercontinuum generation; (060.2390) Fiber optics, infrared; (140.3510) Lasers, fiber; (060.2320) Fiber optics amplifiers and oscillators.

http://dx.doi.org/10.1364/PRJ.4.000135

1. INTRODUCTION

The research on mid-infrared (mid-IR) supercontinuum (SC) sources has drawn worldwide attention because of their great application potential in many areas such as spectroscopy [1], frequency metrology [2], remote sensing [3], and atom physics [4]. In the past decades, SC generation in silica glass fibers [5–13], especially in silica photonic crystal fibers (PCFs) [9–13], has been extensively studied due to the controllable dispersion property and low propagation loss in visible and near-IR regions. Soft glass optical fibers with high nonlinearity and low propagation loss in the mid-IR region, such as chalcogenide [14–17], tellurite [18–20], and fluoride [21–29] glasses, are needed for generating mid-IR SC. Typical fluoride fibers such as ZBLAN (ZrF_4–BaF_2–LaF_3–AlF_3–NaF) fibers, are regarded as competitive candidates for generating high-power mid-IR SC because of the low background loss, relatively high mechanical strength, and commercial availability [29,30]. In 2009, ZBLAN fiber pumped in the 1.55 μm region was demonstrated by Xia *et al.* with an average output power of 10.5 W and a spectrum extending from ~0.8 to 4 μm [23]. ZBLAN fiber pumped by 2 μm pulsed fiber laser was demonstrated to be an attractive option for mid-IR SC generation with the rapid development of the thulium-doped fiber laser (TDFL) [24–28]. A highly efficient SC source pumped by 2 μm TDFL, over 61% of power distribution toward the wavelength longer 3 μm, was demonstrated by Swiderski and Michalska [24]. In 2014, Yang *et al.* demonstrated a high-power SC generation, with 13 W average output power and spectrum extending from ~1.9 to 4.3 μm [25]. Liu *et al.* scaled the average output power up to 24.3 W, while the spectrum spanned just from ~1.9 to 3.3 μm, which is the highest SC output power generated by a ZBLAN fiber [26]. However, it should be noted that mechanical splicing between silica and ZBLAN fibers were utilized in all the systems mentioned above, which actually were not all fibered. The fibers were not permanently jointed together; they were precisely held together by high-precision optical fiber holders. Although the high-precision optical fiber holder is helpful to achieve the high coupling efficiency (~91% in low power operation) [25], it will also raise the cost in the application. And the coupling efficiency obviously will decrease in high-power operation. Because of the low melting temperature of ZBLAN fiber, the tail end of ZBLAN fiber may become bent in high-power operation and cause fiber-core mismatching. This will severely affect the durability and repeatability of the system. Thus, permanent fusion splicing of soft glass fiber and silica fiber is needed for integrated all-fiber robust application. It will promote the practicability and commercial development of the mid-IR SC source. The previous systems were not able to profit fully from the advantages of the fusion splicing between silica fiber and ZBLAN fiber, such as high-power applicability, low Fresnel loss, efficient mode matching, better thermal management, and lack of air interaction [16,31]. Recently, Yin *et al.* demonstrated a mid-IR SC source within a piece of fusion spliced ZBLAN fiber; however, the output average power was only 550.8 mW [32].

In this paper, we demonstrate an all-fiber mid-IR SC source by using a segment of thermal-spliced ZBLAN fiber, with output power up to 10.67 W and spectrum extending from ~1.9 to 4.1 μm. A high-power 1.95 μm master oscillator power amplifier (MOPA) system and a segment of single-mode ZBLAN fiber are used for the mid-IR SC generation. To the best of our knowledge, this is the first high-power integrated

compacted all-fiber mid-IR SC source based on thermal-spliced silica fiber and fluoride fiber.

2. EXPERIMENTAL SETUP AND RESULTS

The seed laser for the MOPA system is a passively mode-locked fiber laser, as schematically shown in Fig. 1. A semiconductor saturable absorber mirror (SESAM) and a fiber Bragg grating (FBG) are used to form a linear cavity. The modulation depth and relaxation time of the SESAM are 20% and ~10 ps, respectively. The FBG acts as a coupling output with 15% transmission at 1950 nm and 3 dB bandwidth of 0.9 nm. A 1560/1950 nm wavelength division multiplexing (WDM) is used to connect the erbium/ytterbium co-doped fiber amplifier (EYDFA) and FBG. The thulium-doped single mode fiber (TSF) is ~11 cm long with core/cladding diameters of 5/125 μm, core numerical aperture (NA) of 0.24, and absorption of ~340 dB/m at 1560 nm. An isolator (ISO) is used to block the backward-propagation light so as to protect the seed laser.

Figure 2 shows the schematic setup of the high-power integrated compacted all-fiber mid-IR SC system. The first-stage single-mode thulium-doped fiber amplifier (TDFA) consists of a 16 W, 793 nm fiber-pigtailed multimode laser diode (LD), a $(2+1)\times 1$ pump combiner, a piece of double-cladding thulium-doped fiber (TDF), a cladding power stripper (CPS), and an ISO. The TDF is ~4 m long with core/cladding diameters of 10/130 μm, core NA of 0.15, and absorption coefficient of 3 dB/m at 793 nm. The CPS is employed to strip unabsorbed cladding light from the TDF for protecting the ISO. After the ISO, a 5:95 coupler is utilized to measure the pulse duration. Between the first and second stage of TDFA, a forward mode field adapter (MFA) is used to connect the coupler and a high-power $(2+1)\times 1$ pump combiner. The input and output fiber of the forward MFA are single-mode fiber (10/130 μm) and large mode area (LMA) fiber (25/250 μm), respectively. Similar to the structure of the single-mode TDFA, the second amplifier stage (LMA TDFA) consists of a 120 W, 793 nm LD, a high-power $(2+1)\times 1$ combiner, an LMA TDF, a high-power CPS, and a backward MFA. The LMA TDF is ~2.5 m long, has core/cladding diameters of 25/250 μm, core NA of 0.09, and absorption of 9.5 dB/m at 793 nm. The input and output fiber of the backward MFA are LMA fiber (25/250 μm) and Nufern SM1950 (7/125 μm), respectively. The backward MFA is used to connect the LMA TDF and single-mode ZBLAN fiber. The single-mode ZBLAN fiber is ~8 m long with core/cladding diameters of 9/125 μm and core NA of 0.2. The zero-dispersion wavelength of the ZBLAN fiber is ~1.57 μm. The output end of the ZBLAN fiber is cleaved with an angle of 8° to avoid backward-propagation light. A thermal splicing method is utilized to connect the single-mode ZBLAN fiber and the SM1950 fiber with a splicing loss of 0.96 dB.

In our experiment, the time-domain characteristics of the system are measured by a digital oscilloscope (Tektronix, DPO 7104C, 1 GHz), a high-speed InGaAs photodetector (EOT, ET-5000, 12.5 GHz), and an autocorrelator (APE, pulseCheck USB). A high-power thermal power meter is utilized to measure the output power. An optical spectrum analyzer (YOKOGAWA, AQ 6375, 1200–2400 nm) is used to measure the output spectrum from ~1.9 to 2.4 μm, and a Fourier transform IR spectroscopy (Bruker, Tensor 27) is used to measure the longer wavelength with resolutions of 0.05 and 0.3 nm, respectively.

The spectrum of the passively mode-locked fiber laser is shown in Fig. 3. The central wavelength and 3 dB bandwidth are 1950 and 0.148 nm, respectively. The pulse train of the passively mode-locked fiber laser is shown in Fig. 4(a) with a pulse repetition rate of 75.4 MHz. Figure 4(b) shows the corresponding RF spectrum with a span of 2 GHz and resolution of 3 kHz. The inset of Fig. 4(b) gives an SNR of ~65 dB at the fundamental rate of ~75.4 MHz, which indicates that the seed laser is operating at a stable state. The maximum output power of the seed laser is ~25 mW. Due to the low output power of the seed laser, the pulse duration could not be measured by the autocorrelator (APE, pulseCheck USB). Therefore, the pulse duration is measured at the 5% output port of the coupler after the first-stage amplifier, and the measured FWHM pulse duration is 12.58 ps, as shown in the inset in Fig. 4(a). The maximum output power of the first stage is ~2.4 W without obvious spectral broadening. When the power is further boosted in the LMA TDFA, the laser spectrum obviously broadens at the output port of the backward MFA. This is mainly caused by self-phase modulation, modulation instability (MI), and stimulated Raman scattering (SRS) because of the increasing pulse peak power [22].

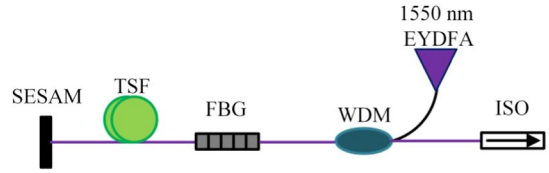

Fig. 1. Schematic setup of the passively mode-locked fiber laser.

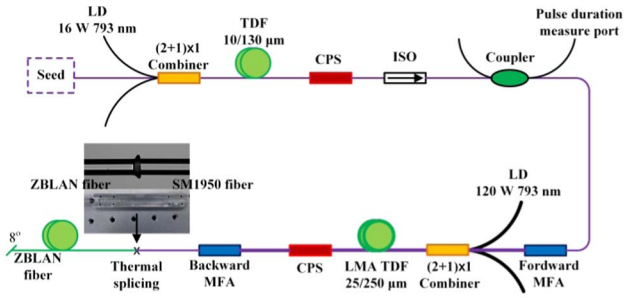

Fig. 2. Schematic setup of the high-power integrated compacted all-fiber mid-IR SC system.

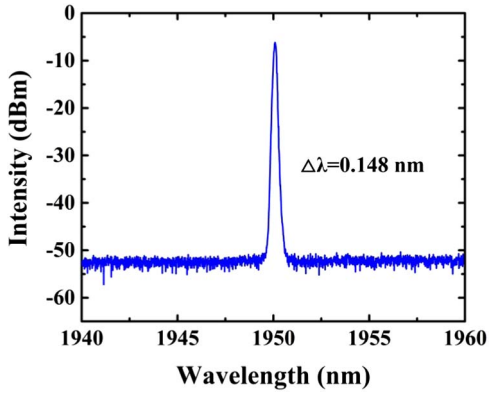

Fig. 3. Spectrum of the mode-locked fiber laser.

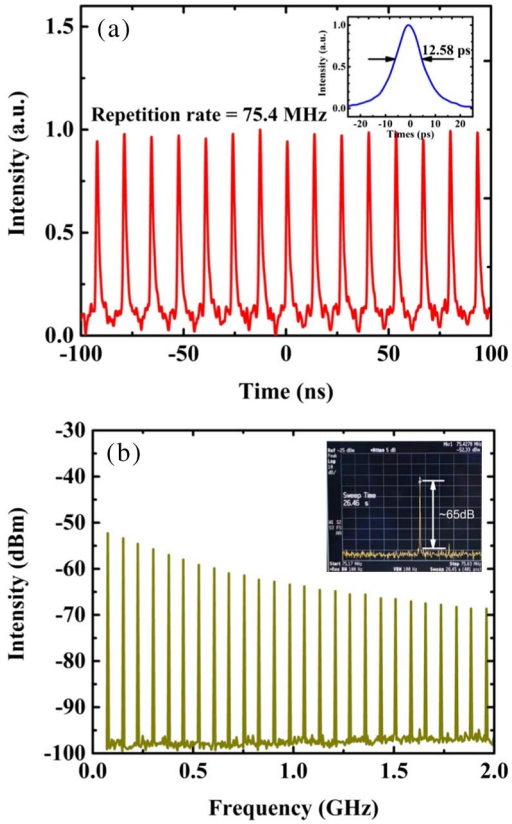

Fig. 4. (a) Pulse train of the passively mode-locked fiber with a repetition of 75.4 MHz. Inset: the pulse autocorrelation trace of the first amplifier at average output power of 100 mW. (b) RF spectrum of harmonic repetition rate within 2 GHz. Inset: the RF spectrum around fundamental repetition rate.

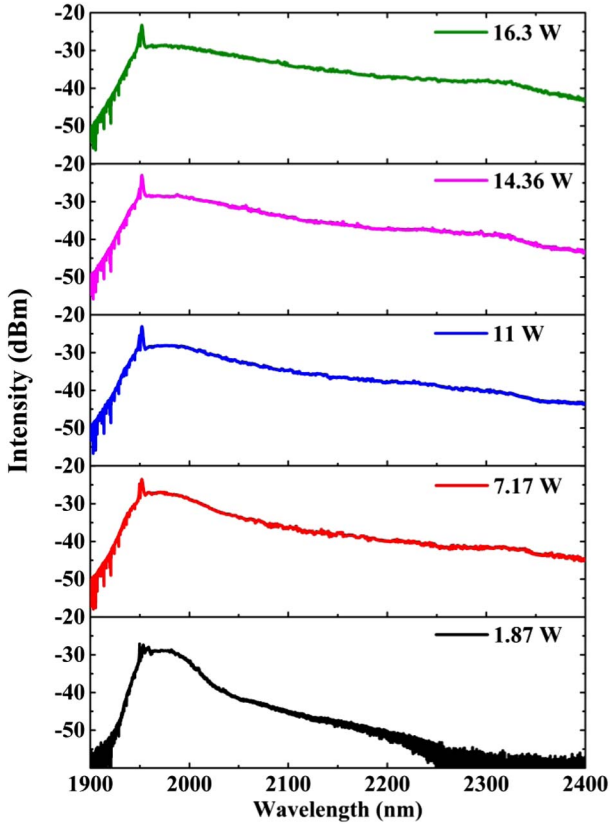

Fig. 5. Output spectra of the backward MFA at different average output power.

Figure 5 shows the output spectra from the backward MFA at different output powers, which extend to beyond 2.4 μm when the output power of the backward MFA is increased up to 7.17 W and more. Obviously, spectrum broadening is not observed when further increase the pump power due to the high intrinsic attenuation of the silica fiber at long wavelength.

Permanent splicing is the key technique to realize an integrated all-fiber system. The pigtailed SM1950 fiber of the backward MFA is connected with the single-mode ZBLAN fiber by thermal splicing. Fibers are fixed on a commercial splicer (Vytan GPX-3000) after end faces are flat cleaved. Several times of manual alignments are set to reduce the butt-coupling loss of the two fibers because of the slightly eccentric of the ZBLAN fiber core. Due to the distinct difference of the two fibers' melting temperature, an offset splicing method is needed to ensure more heat is applied to the SM1950 fiber; finally, a splicing loss of 0.96 dB is achieved. The bulged ZBLAN fiber wrapping around the SM1950 fiber confirms that the two different fibers are thermal-spliced together. Effective thermal management is quite necessary because the ZBLAN fiber could be damaged by the thermal effect in high-power operation. Therefore, the splicing joint is covered with high-index UV adhesive and packaged into an aluminum groove after curing, as shown in the inset of the Fig. 2. Then, the aluminum groove is fixed on a water-cooled heat sink for better thermal management. The rest of the ZBLAN fiber is placed on another heat sink, with which the temperature is set a little higher than the previous one because of its low resistance to moisture. The output end of the ZBLAN fiber is cleaved with an angle of ~8° to avoid Fresnel reflection. The power capacity of the splicing joint is tested using the same method as illustrated in [31]. With increasing of the input power, the output power also increases linearly. This shows that the splicing loss of the two fibers keeps stable. This work also indicates important application potential for integrated high-power all-fiber mid-IR SC generation.

Figure 6 shows the output spectra from the ZBLAN fiber at different output powers. The MI generated in the LMA TDFA can break the long pulses into short pulses and create solitons. The solitons further propagate along the ZBLAN fiber and lead to a soliton self-frequency shift with the spectrum further broadening at the output port of the ZBLAN fiber [30]. The 20 dB bandwidth of the spectrum is ~1.9 to 4.1 μm at the maximum average output power of 10.67 W. The typical dip at ~2.8 μm can be seen on the output spectra, which is caused by the intrinsic H_2O absorption of the ZBLAN fiber. Two other dips, at around 3.2 and 3.6 μm, respectively, would be caused by some inconclusive reasons during the measure process. In [25], Yang also has observed a similar phenomenon.

Figure 7 shows the different output powers from the LMA TDFA, backward MFA, ZBLAN fiber, and the temperature of the splicing joint. The maximum output power of LMA TDFA, backward MFA, and ZBLAN fiber are 42.7, 16.3, and 10.67 W, respectively. The slope efficiency of the LMA TDFA is ~37%, which can be further improved by optimizing the length of the gain fiber of the system. And the transmission

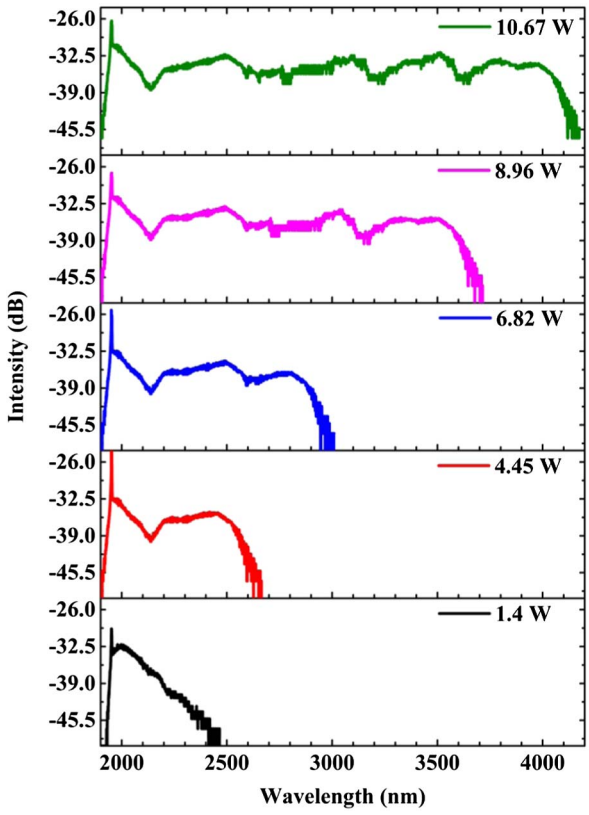

Fig. 6. Output spectra from the ZBLAN fiber at different average output power.

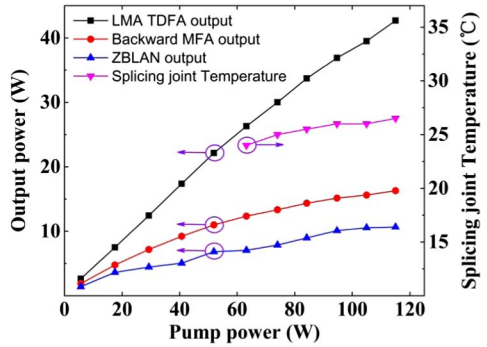

Fig. 7. Different output powers and splicing joint temperature versus the pump power of LMA TDFA.

efficiency of the backward MFA decreases obviously because of the wavelength-dependent insert loss of the backward MFA, high intrinsic attenuation of the silica fiber beyond ~2.7 μm, and spectral broadening. It decreases from ~71% to ~38% when the output power of the LMA TDFA increases from 2.63 to 42.7 W. The conversion efficiency of mid-IR SC generation is ~65.5% with respect to the backward MFA output power at the maximum pump power. When increasing the pump power up to 115 W, the temperature of the splicing joint rises steadily to 26.5°C; this also indicates that sufficient thermal management is necessary for high-power operation. The slope efficiency of SC output power from ZBLAN fiber also decreases, which is mainly caused by the spectrum broadening. It is worth noting that the mechanical coupling efficiency is sensitive during the core aligning process and always decreases in high-power operation. Compared with mechanical splicing, permanent thermal splicing of these two fibers not only enhances the robustness and practicability of the system but also improves the reproducibility and thermal management capability. In future work, we will concentrate on the stability of the system such as optimizing the TDFA, reducing the splicing loss, and employing the fluoride end-cap.

3. CONCLUSION

In conclusion, an integrated high-power all-fiber mid-IR SC system is demonstrated. The achieved maximum mid-IR SC power is 10.67 W with a wavelength spanning from ~1.9 to 4.1 μm. The high-power integrated compacted all-fiber mid-IR SC system would be suitable for practical applications. This mid-IR SC source, to the best of our knowledge, is the first high-power real-all-fiber-format system that benefits from our in-house-developed thermal splicing technology for splicing typical silica and ZBLAN fibers.

Funding

National High-tech R&D Program of China (863 Program) (2015AA021102); Innovative Research and Development Project of Nanshan District (KC2013JSCX0013A); China Postdoctoral Science Foundation (2015M572353, 2015M582407); Natural Science Foundation of SZU (201457); National Natural Science Foundation of China (NSFC) (61275144, 61308049); Science and Technology Projects of Shenzhen City (JCYJ20130329103213543, JCYJ20140418091413568, JCYJ20150324140036862).

REFERENCES

1. M. Kumar, M. N. Islam, F. L. Terry, M. J. Freeman, A. Chan, M. Neelakandan, and T. Manzur, "Stand-off detection of solid targets with diffuse reflection spectroscopy using a high-power mid-infrared supercontinuum source," Appl. Opt. **51**, 2794–2807 (2012).
2. C. H. Li, A. G. Glenday, A. J. Benedick, G. Q. Chang, L. J. Chen, C. Cramer, P. Fendel, G. Furesz, F. X. Kärtner, S. Korzennik, D. F. Phillips, D. Sasselov, A. Szentgyorgyi, and R. L. Walsworth, "In-situ determination of astro-comb calibrator lines to better than 10 cm^{-1}," Opt. Express **18**, 13239–13249 (2010).
3. V. V. Alexander, Z. Shi, M. N. Islam, K. Ke, G. Kailinchenko, M. J. Freeman, A. Ifarraguerri, J. Meola, A. Absi, J. Leonard, J. A. Zadnik, A. S. Szalkowski, and G. J. Boer, "Field trial of active remote sensing using a high-power short-wave infrared supercontinuum laser," Appl. Opt. **52**, 6813–6823 (2013).
4. C. Vozzi, M. Negro, and S. Stagira, "Strong-field phenomena driven by mid-infrared ultrafast sources: JMO Series: attosecond and strong field science," J. Mod. Opt. **59**, 1283–1302 (2012).
5. C. Lin and R. H. Stolen, "New nanosecond continuum for excited-state spectroscopy," Appl. Phys. Lett. **28**, 216–218 (1976).
6. P. G. Yan, J. Shu, S. C. Ruan, J. Zhao, J. Q. Zhao, C. L. Du, C. Y. Guo, H. F. Wei, and J. Luo, "Polarization dependent visible supercontinuum generation in the nanoweb fiber," Opt. Express **19**, 4985–4990 (2011).
7. R. Song, J. Hou, S. P. Chen, W. Q. Yang, and Q. S. Lu, "High power supercontinuum generation in a nonlinear ytterbium-doped fiber amplifier," Opt. Lett. **37**, 1529–1531 (2012).
8. J. Swiderski and M. Michalska, "Mid-infrared supercontinuum generation in a single-mode thulium-doped fiber amplifier," Laser Phys. Lett. **10**, 035105 (2013).
9. X. H. Fang, M. L. Hu, L. L. Huang, L. Chai, N. L. Dai, J. Y. Li, A. Y. Tashchilina, A. M. Zheltikov, and C. Y. Wang, "Multiwatt octave-spanning supercontinuum generation in multicore photonic-crystal fiber," Opt. Lett. **37**, 2292–2294 (2012).

10. K. M. Hilligse, T. V. Andersen, H. N. Paulsen, C. K. Nielsen, K. Mlmer, S. Keiding, R. Kristiansen, K. P. Hansen, and J. J. Larsen, "Supercontinuum generation in a photonic crystal fiber with two zero dispersion wavelengths," Opt. Express **12**, 1045–1054 (2004).
11. H. W. Chen, S. P. Chen, J. H. Wang, Z. L. Chen, and J. Hou, "35 W high power all fiber supercontinuum generation in PCF with picosecond MOPA laser," Opt. Commun. **284**, 5484–5487 (2011).
12. J. M. Dudley, G. Genty, and S. Coen, "Supercontinuum generation in photonic crystal fiber," Rev. Mod. Phys. **78**, 1135–1184 (2006).
13. P. G. Yan, G. L. Zhang, H. F. Wei, D. Q. Ouyang, S. S. Huang, J. Q. Zhao, K. K. Chen, J. Luo, and S. C. Ruan, "Double cladding seven-core photonic crystal fibers with different GVD properties and fundamental supermode output," J. Lightwave Technol. **31**, 3658–3662 (2013).
14. L. B. Shaw, P. A. Thielen, F. H. Kung, V. Q. Nguyen, J. S. Sanghera, and I. D. Aggarwal, "IR supercontinuum generation in As-Se photonic crystal fiber," in *Advanced Solid-State Photonics (ASSP)* (Optical Society of America, 2005).
15. P. G. Yan, R. J. Dong, G. L. Zhang, H. Q. Li, and S. C. Ruan, "Numerical simulation on the coherent time-critical 2–5 μm supercontinuum generation in an As_2S_3 microstructured optical fiber with all-normal flat-top dispersion profile," Opt. Commun. **293**, 133–138 (2013).
16. R. Thapa, R. R. Gattass, V. Nguyen, G. Chin, D. Gibson, W. Kim, L. B. Shaw, and J. S. Sanghera, "Low-loss, robust fusion splicing of silica to chalcogenide fiber for integrated mid-infrared laser technology development," Opt. Lett. **40**, 5074–5077 (2015).
17. C. R. Petersen, U. Møller, I. Kubat, B. Zhou, S. Dupont, J. Ramsay, T. Benson, S. Sujecki, N. Abdel-Moneim, Z. Tang, D. Furniss, A. Seddon, and O. Bang, "Mid-infrared supercontinuum covering the 1.4–13.3 μm molecular fingerprint region using ultra-high NA chalcogenide step-index fibre," Nat. Photonics **8**, 830–834 (2014).
18. R. Thapa, D. Rhonehouse, D. Nguyen, K. Wiersma, C. Smith, J. Zong, and A. Chavez-Pirson, "Mid-IR supercontinuum generation in ultra-low loss, dispersion-zero shifted tellurite glass fiber with extended coverage beyond 4.5 μm," Proc. SPIE **8898**, 889808 (2013).
19. P. Domachuk, N. A. Wolchover, M. Cronin-Golomb, A. Wang, A. K. George, C. M. B. Cordeiro, J. C. Knight, and F. G. Omenetto, "Over 4000 nm bandwidth of mid-IR supercontinuum generation in sub-centimeter segments of highly nonlinear tellurite PCFs," Opt. Express **16**, 7161–7168 (2008).
20. M. Belal, L. Xu, P. Horak, L. Shen, X. Feng, M. Ettabib, D. J. Richardson, P. Petropoulos, and J. H. V. Price, "Mid-infrared supercontinuum generation in suspended core tellurite microstructured optical fibers," Opt. Lett. **40**, 2237–2240 (2015).
21. C. L. Hagen, J. W. Walewski, and S. T. Sanders, "Generation of a continuum extending to the midinfrared by pumping ZBLAN fiber with an ultrafast 1550-nm source," IEEE Photon. Technol. Lett. **18**, 91–93 (2006).
22. K. Liu, J. Liu, H. Shi, F. Tan, and P. Wang, "High power mid-infrared supercontinuum generation in a single-mode ZBLAN fiber with up to 21.8 W average output power," Opt. Express **22**, 24384–24391 (2014).
23. C. Xia, Z. Xu, M. N. Islam, F. L. Terry, Jr., M. J. Freeman, A. Zakel, and J. Mauricio, "10.5 W time-averaged power mid-IR supercontinuum generation extending beyond 4 μm with direct pulse pattern modulation," IEEE J. Sel. Top. Quantum Electron. **15**, 422–434 (2009).
24. J. Swiderski and M. Michalska, "High-power supercontinuum generation in a ZBLAN fiber with very efficient power distribution toward the mid-infrared," Opt. Lett. **39**, 910–913 (2014).
25. W. Q. Yang, B. Zhang, G. H. Xue, K. Yin, and J. Hou, "Thirteen watt all-fiber mid-infrared supercontinuum generation in a single mode ZBLAN fiber pumped by a 2 μm MOPA system," Opt. Lett. **39**, 1849–1852 (2014).
26. K. Liu, J. Liu, H. Shi, F. Tan, and P. Wang, "24.3 W mid-infrared supercontinuum generation from a single-mode ZBLAN fiber pumped by thulium-doped fiber amplifier," in *Advanced Solid State Lasers (ASSL)* (Optical Society of America, 2014).
27. J. Swiderski, M. Michalska, and G. Maze, "Mid-IR supercontinuum generation in a ZBLAN fiber pumped by a gain-switched mode-locked Tm-doped fiber laser and amplifier system," Opt. Express **21**, 7851–7857 (2013).
28. M. Eckerle, C. Kieleck, J. Swiderski, S. D. Jackson, G. Maze, and M. Eichhorn, "Actively Q-switched and mode-locked Tm^{3+}-doped silicate 2 μm fiber laser for supercontinuum generation in fluoride fiber," Opt. Lett. **37**, 512–514 (2012).
29. X. Zhu and N. Peyghambarian, "High-power ZBLAN glass fiber lasers: review and prospect," Adv. Optoelectron. **2010**, 501956 (2010).
30. J. Swiderski, "High-power mid-infrared supercontinuum sources: current status and future perspectives," Prog. Quant. Electron. **38**, 189–235 (2014).
31. Z. J. Zheng, D. Q. Ouyang, J. Q. Zhao, S. C. Ruan, J. Yu, C. Y. Guo, and J. Z. Wang, "An effective thermal splicing method to join fluoride and silica fibers for a high power regime," Chin. Phys. Lett. **32**, 114206 (2015).
32. K. Yin, B. Zhang, J. Yao, L. Yang, S. Chen, and J. Hou, "Highly stable, monolithic, single-mode mid-infrared supercontinuum source based on low-loss fusion spliced silica and fluoride fibers," Opt. Lett. **41**, 946–949 (2016).